Conformational Polymorphism of Wild-Type and Mutant Prion Proteins: Energy Landscape Analysis

Yaakov Levy* **and Oren M. Becker**
Department of Chemical Physics, School of Chemistry, Tel Aviv University, Tel Aviv, Israel

ABSTRACT **Conformational transitions are thought to be the prime mechanism of prion diseases. In this study, the energy landscapes of a wild-type prion protein (PrP) and the D178N and E200K mutant proteins were mapped, enabling the characterization of the normal isoforms (PrP^{C}) and partially unfolded isoforms (PrP^{PU}) of the three prion protein analogs. It was found that the three energy landscapes differ in three respects: (i) the relative stability of the PrP^{C} and the PrP^{PU} states, (ii) the transition pathways from PrP^{C} to PrP^{PU}, and (iii) the relative stability of the three helices in the PrP^{C} state. In particular, it was found that although helix 1 (residues 144-156) is the most stable helix in wild-type PrP, its stability is dramatically reduced by both mutations. This destabilization is due to changes in the charge distribution that affects the internal salt bridges responsible for the greater stability of this helix in wild-type PrP. Although both mutations result in similar destabilization of helix 1, they a have different effect on the overall stability of PrP^{C} and of PrP^{PU} isoforms and on structural properties. The destabilization of helix 1 by mutations provides additional evidences to the role of this helix in the pathogenic transition from the PrP^{C} to the pathogenic isoform PrP^{SC}. Proteins 2002;47:458–468.** © 2002 Wiley-Liss, Inc.

Key words: conformational transitions; wild-type prion proteins; D178N PrP mutant; E200K PrP mutant; energy landscape

INTRODUCTION

Prion diseases, also known as transmissible spongiform encephalopathies, are sporadic, inherited, or infectious mammalian neurodegenerative disorders. These include Creutzfeld-Jacob disease (CJD), Gerstmann-Straussler-Scheinker syndrome (GSS), and fatal familial insomnia (FFI) in humans as well as sheep scrapie, mink encephalopathy, and bovine spongiform encephalopathy [BSE ("mad cow" disease)].[1–3] Common to these diseases are pathogenic modifications in prion proteins (PrP), which in normal cells are nonpathogenic. A large body of data accumulated so far supports the "protein-only" hypothesis for prion diseases,[2,4] although some investigators support a virus-like mechanism.[5,6]

The protein-only hypothesis[2,4] suggests that prion infection is associated with a conformational transition between the normal cellular form of the prion protein, PrP^{C}, and an abnormal infectious form, PrP^{SC}. Spectroscopic measurements showed marked structural differences between the two PrP isoforms. Although PrP^{C} contains 42% α-helix and only 3% β-sheet, the abnormal PrP^{SC} is composed of 30% α-helix and 43% β-sheet.[7] Other studies have indicated that in its amyloid precursor state, the PrP has characteristics of a molten globule with an intrinsically unstable tertiary structure.[8] Recently, the monomeric three-dimensional structures of the PrP^{C} conformer of four PrPs (mouse,[9,10] Syrian hamster,[11] bovine,[12] and human PrP[13]) were determined by NMR. In all cases, the N-termini were highly flexible, lacking an identifiable secondary structure. The rest of the molecules (residues 121–231 in mice, 113–231 in hamsters, 121–230 in bovine, and 125–228 in humans) had similar, although not identical, structures consisting of one short helix (helix 1) and two long helices (helices 2 and 3) linked by a disulfide bond.

The mechanism by which PrP^{C} converts to PrP^{SC} is unknown, although two major models have been proposed.[14] The standard catalytic model[15] proposes that monomeric PrP^{C} is spontaneously converted to a rare partially unfolded conformation designated PrP*. When the PrP gene is mutated, or on infection with PrP^{SC}, the transitional PrP* conformation, with or without accessory molecules (e.g., protein X[16]), binds to monomeric PrP^{SC}, which then stimulates the conversion of PrP* to PrP^{SC}. Alternatively, the nucleated polymerization model[17,18] proposes that PrP^{SC} is intrinsically multimeric, differing from PrP^{C} primarily in its quaternary structure. Changes in secondary and tertiary structures may accompany this change in the polymerization state, as seems to occur with amyloid formation.[19]

The uncertainty about the mechanism of the PrP structural transition is to a large extent due to the fact that the structures of the PrP* conformer and the abnormal PrP^{SC} conformer are unknown. A model for the tertiary structure of PrP^{SC} was suggested,[20] but so far there is no direct experimental support for it.

Several mutations that cause inherited prion diseases have been found throughout the prion protein. Because all of the known biologically significant PrP point mutations occur either within or adjacent to regions of secondary structure, it was assumed that these amino acid substitu-

Grant sponsor: Clore Foundation.

O.M. Becker's current address is Bio Information Technologies (Bio IT) Ltd., S.H.P. Building, 3 Hayetzira St., Ramat Gan 52521, Israel.

*Correspondence to: Y. Levy, School of Chemistry, Tel-Aviv University, Tel-Aviv 69978, Israel. E-mail: kobylevy@post.tau.ac.il

Received 11 May 2001; Accepted 21 December 2001

tions destabilize the structure of PrP^C and facilitate its transition into PrP^{SC}.[4,21] Recently, on the basis of the NMR structure of wild-type mouse PrP, it was suggested that mutations may indeed reduce the stability of the PrP^C form by inducing loss of internal hydrogen bonds and salt bridges.[22] Furthermore, in a previous study, we found that the A117V mutation, which is linked to GSS disease, significantly destabilizes the helix conformation of the pathogenic PrP106-126 peptide, leading to complete loss of helicity by approximately 1 ns faster than in the wild-type.[32] However, it was proposed that destabilization of PrP^C by point mutation is not always valid and that these mutations have a minor effect on the protein stability.[22] Namely, the amino acid exchanges that are linked with inherited prion diseases destabilize PrP^C differently, depending on their spatial position and on the intramolecular interactions in which they participate.

The two-point mutations, D178N and E200K, selected for the present study were chosen from among the many mutations known to be associated with inherited prion diseases. The selection was based on their biological and chemical properties, as well as on their spatial locations in the PrP^C structure. Specifically, both D178N and E200K mutations cause spontaneous appearance of CJD.[24–26] Moreover, both mutations induce changes in partial charges. In the D178N mutation, a change occurred from a positively charged residue (Asp) to an uncharged hydrophilic residue (Asn), and in the E200K mutation, a change occurred from a negatively charged residue (Glu) to a positively charged residue (Lys). Figure 1 shows the NMR structure of mouse PrP^C and the sites of the two-point mutations. Residue 178 is located in helix 2 and is stabilized by a hydrogen bond to Tyr128 and by a salt bridge to Arg164. Residue 200 is located at the protein surface in the loop connecting helices 2 and 3. Therefore, the different structural locations of these two residues suggest different effects on the stability of PrP^C. Accordingly, the D178N mutation may result in changes to the hydrogen network and loss of a salt bridge, thus destabilizing the structure of PrP^C. On the other hand, the location of E200 on the protein surface may suggest that the E200K mutation does not have a major impact on the stability of PrP^C.

In recent years, several molecular dynamic (MD) simulations were performed to complement experiments and to characterize the atomic level conformational properties of the $PrP^C \rightarrow PrP^{SC}$ conversion.[27–31] For example, molecular dynamics was used to explore the conformational flexibility of PrP^C,[31] the effects of low pH,[30] and the effect of point mutations[31] on the dynamics and stability of the prion protein. In all these studies, the PrP^{SC} isoform was not detected, and only small changes in the secondary structure content of PrP^C were found. The lack of additional β-structures in these simulations may originate from current computational limitations that restrict the simulation time to a few nanoseconds when introducing the water explicitly. To overcome this limitation and to explore the dynamical properties of PrP^C more extensively, we study here the prion unfolding process by simulating a wild-type PrP^C at relatively high temperatures (350–500 K) by using an implicit solvent

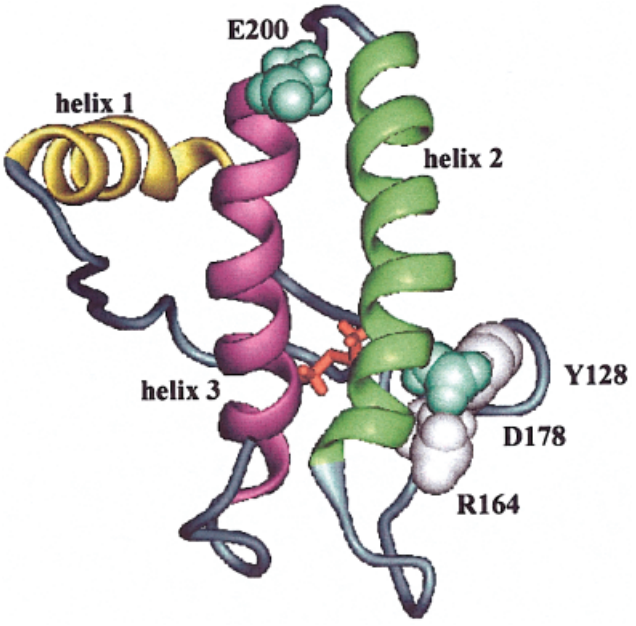

Fig. 1. The NMR structure of mouse PrP^C (PDB entry 1AG2, which includes residues 124–226). Helix 1 (residues 144–153), helix 2 (residues 172–194), and helix 3 (residues 200–224) are marked in yellow, green, and pink, respectively. The disulfide bond (Cys179-Cys214) that bridges helix 2 and helix 3 is shown in red. The side-chains of Asp(D)178 and Glu(E)200 are shown by green vdW spheres. The side-chains of Arg(R)164 and Tyr(Y)128, which form a salt bridge and a hydrogen bond with D178, are shown by gray vdW spheres.

model. The unfolding process of D178N and E200K mutant PrP were also explored in an attempt to rationalize their relative tendency toward the disease. To correlate stability (energy) with structure (secondary structural elements) along the unfolding routes for the three prion proteins, their underlying energy landscapes were constructed respectively.

It is known that the conformational properties of PrP, like those of any other protein, are determined by the underlying energy landscape,[32–34] in which different regions reflect different PrP isoforms. The size and depth of the respective regions of the landscape determine the relative thermodynamic stability of the conformers. In this study, we generate detailed quantitative maps of the energy landscapes of wild-type mouse PrP and of its D178N and E200K mutants in aqueous solution. Previously, we constructed the energy landscape of wild-type mouse PrP in a hydrophobic environment (vacuum calculation).[35] The energy landscapes of wild-type PrP and of its two mutants may enable us to characterize their partially unfolded isoforms, the transition pathways from PrP^C to these isoforms, and the effect of the mutation on the PrP isoforms as well as on the mechanism of structural conversion. The properties of the unfolding process obtained from the present study of monomeric PrPs may also enable us to infer about the protein multimerization process.

MATERIALS AND METHODS

The energy landscape of PrP was constructed with a procedure previously developed for polypeptide sys-

tems.[36–38] Starting from the NMR structure of mouse (which includes residues 124–226[9,10]), a total sample of 600 conformations was collected from four high-temperature molecular dynamics trajectories. High temperatures are required to explore the PrP polymorphism because the overall structure of PrP remains unchanged during 1- and 2-ns molecular dynamics at 300 K.[29,31] Specifically, two 1-ns trajectories simulated at 350 K and 400 K each and two 2-ns trajectories simulated at 450 K and 500 K each resulted in a total of 6-ns simulation times for the wild-type PrP. Sets of 100 and 200 conformations were collected at equal intervals from each of the 1-ns and 2-ns trajectories, respectively. Each conformation that was collected from the sampling trajectories was gradually cooled down to 300 K and then minimized to the nearest local minimum. All simulations were performed with the molecular dynamics program CHARMM[39] and the charmm27 force field,[40] using 2-fs timesteps and 10 Å cutoff.

The simulations were performed with the EEF1 implicit solvent model,[41] which expresses the solvation-free energy as a sum over group contributions, where the solvation-free energy of each group is corrected for the screening by surrounding groups in the first solvation shell. This model uses neutralized ionic side-chains and a linear distance-dependent dielectric function to simulate the shielding effects of water on electrostatic interaction, eliminating long-range electrostatic interactions. The EEF1 model has been shown to give good results for the folding[42–44] and unfolding[45,46] processes of various proteins and is able to discriminate between native and misfolded protein structures.[47–49] Moreover, simulations using this model have been shown to yield a good agreement with explicit solvent simulations. For example, the root-mean-square deviations (RMSDs) from experimental structures,[41] the thermal unfolding pathways,[50] and the destabilization of helical polyalanines in aqueous solution[51], as calculated by the EEF1 model, are similar to those obtained from explicit solvent simulations. In a recent study, similar results were obtained for the effect of a single point mutation (A117V) and of an acidic pH on the rates of the helix-coil transition of the fragment PrP106-126 using the EEF1 and explicit solvent models.[23] Both models indicate that the mutation and an acidic pH increase the transition rates compared with the wild-type and differ only in the absolute values of the rates, observation that can be attributed to the different solvent response in the implicit and explicit models.

A 600 × 600 matrix of pairwise backbone RMS distances between all of the conformations was compiled. A variant of the principal component analysis technique[36,37] was used to project the high-dimensional molecular conformation space of PrP onto a low dimensional subspace. Because of the large conformation transition undergone by PrP, even the two principal coordinates yield a qualitatively accurate projection[36] in this case (the 2D projections capture 45–50% of the normalized sum of all eigenvalues, and the 3D projections capture 56–60% of that sum for the three PrP analogs). The "minimal energy envelope" procedure,[36] which is equivalent to adiabatic mapping,[52] was used to highlight the underlying landscape topography (without the barriers).

The same procedure was applied to construct the energy landscapes of D178N and E200K mutants (i.e., based on a total of 6-ns simulation times for each mutant protein). The initial conformations of the D178N and E200K PrP mutants were constructed by substituting Asp → Asn at position 178 and Glu → Lys at position 200, respectively, followed by 200 steps of steepest descent minimization.

The α-helix and β-sheet content of each sampled conformation for each of the three prions was calculated by using the DSSP program.[53] The maximal length for each of the three PrP^C helices was determined as the maximal length encountered in any of the conformations sampled for either the wild-type PrP or for its mutants. Thus, we define that helix 1 is composed at most of 13 residues (residues 144–156), that the maximal length of helix 2 is 23 residues (residues 172–194), and that the length of helix 3 is at most 22 residues (residues 200–221). The specific lengths of the three PrP^C helices in each conformation were computed relative to these maximal lengths. It should be noted that the lengths of helices 1 and 3 of mouse PrP^C, as determined by NMR[9,10] (span residues 144–153 and 200–218, respectively), are three residues shorter than those found by molecular dynamics simulations.

RESULTS AND DISCUSSION

Energy Landscapes of Wild-Type, D178N, and E200K Mutants PrP

Figure 2 depicts the resulting energy landscapes for the wild-type, D178N, and E200K mutant mouse PrP. In these pictures, the potential energy is shown as a function of conformational similarity and is represented by the projection on the two main principal coordinates of the system, q_1 and q_2. The three energy landscapes include the native PrP^C conformation basin designated by an asterisk, as well as partially unfolded PrP conformations, which we designate as PrP^{PU}. An expected region in the energy landscape, associated with the pathogenic conformation PrP^{SC}, was not mapped, probably because the sampling procedure that was used could not overcome the high barriers separating PrP^{SC} from the rest of the landscape. Alternative reasons for not observing PrP^{SC} may be because this isoform does not exist as a monomer, or because it is stable only in the presence of the long flexible prion N-terminal region (residues 1–122).[9,10]

Two transition pathways, connecting PrP^C to the partially unfolded PrP conformations, are seen on the energy landscape of wild-type PrP [Fig. 2(a)]. The α-helical content for all 600 sampled conformations of wild-type PrP, projected on the same two principal coordinates used in Figure 2(a), (q_1 and q_2), is shown in Figure 3(a). This figure clearly reflects the structural difference between PrP^C and the partially unfolded PrP conformations. Starting from the highly α-helical PrP^C isoform, the α-helical content decreases gradually along both pathways from 49.5 to 15.2% along pathway I and to 35.6% along pathway II. Namely, the decrease along pathway II is much smaller than that along pathway I, indicating mostly different orientations of the three helices compared to significant unwinding of the helices along pathway I.

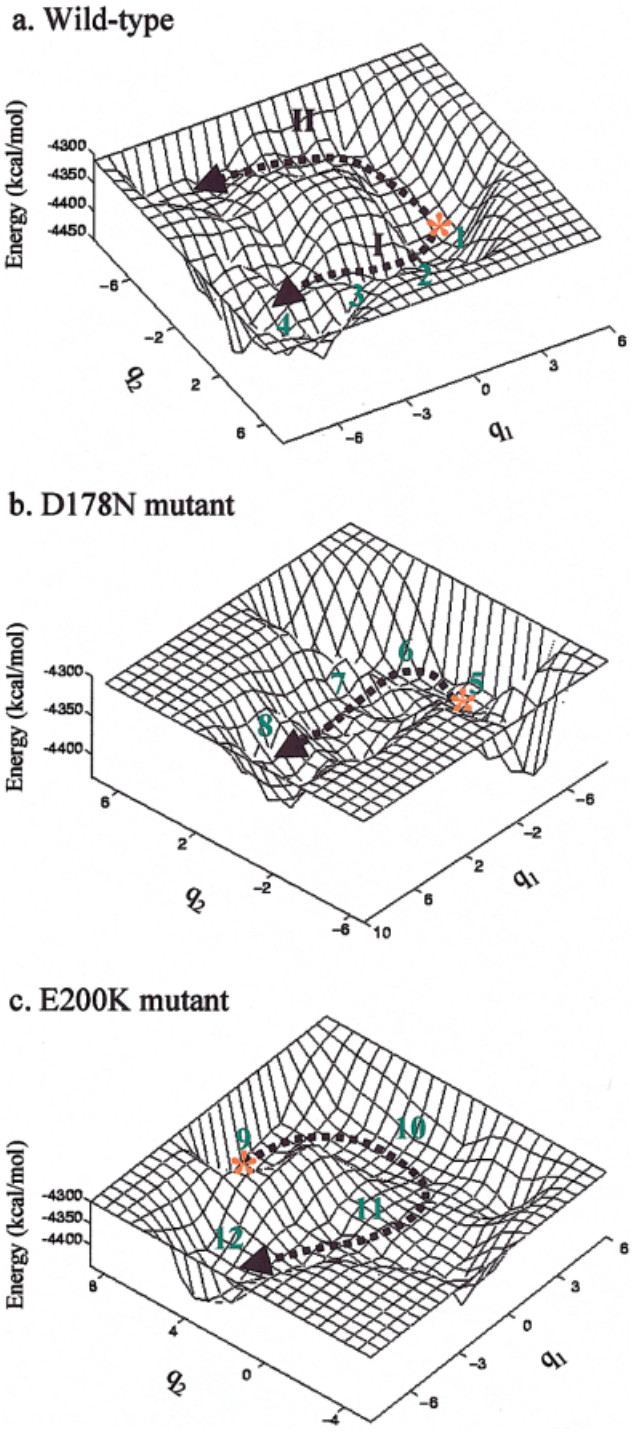

Fig. 2. The energy landscapes of (**a**) wild-type mouse prion protein, (**b**) D178N mutant, and (**c**) E200K mutant. The three prion proteins include residues 124–226. The potential energy is shown as a function of the two first principal axes, q_1 and q_2, representing conformational similarity. Arrows indicate transition regions connecting the PrP^{C} isoform (designated by an asterisk) and the less stable, partially unfolded, PrP^{PU} conformations. Although the energy landscape of wild-type PrP includes two transition pathways, I and II, both D178N and E200K mutant energy landscapes exhibit only a single pathway. Points 1–4, 5–8, and 9–12 indicate sample conformations along these pathways and serve as a reference for Figure 5.

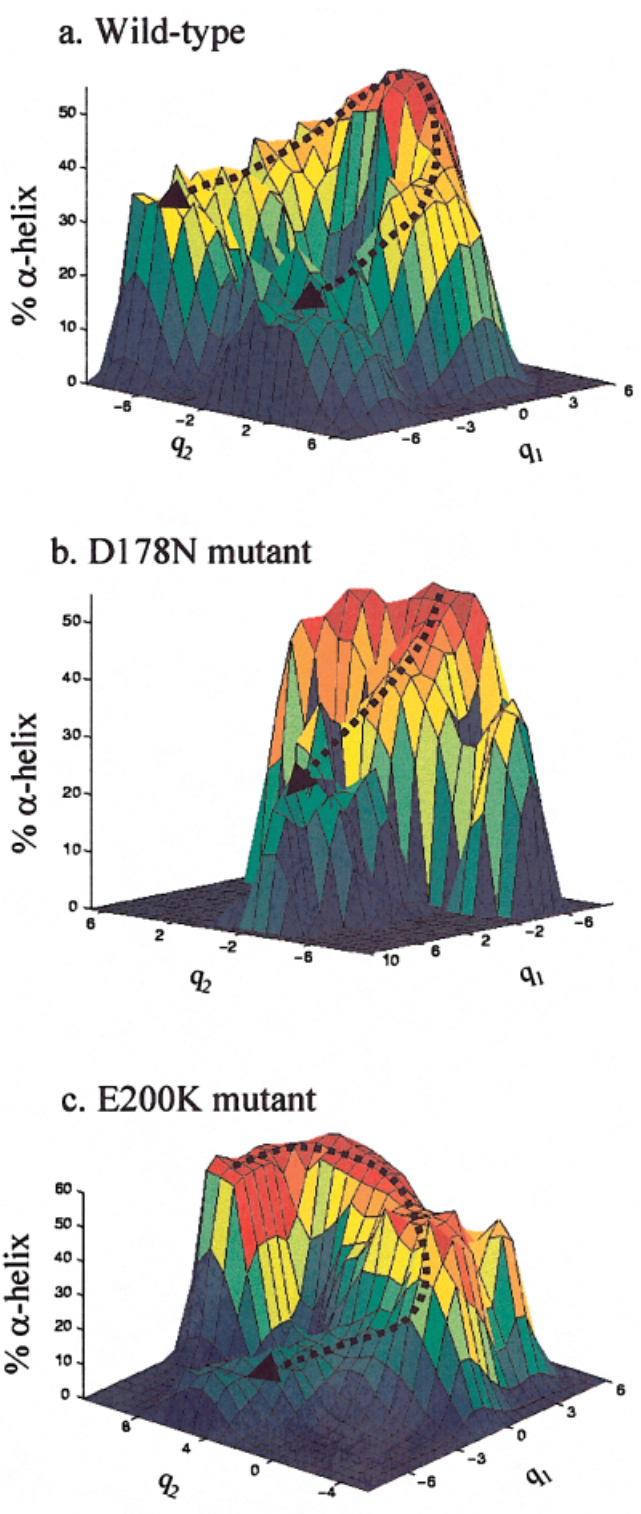

Fig. 3. The percentage of α-helical content for all sampled conformations of (**a**) wild-type PrP, (**b**) D178N mutant, and (**c**) E200K mutant, projected on the same two principal coordinates, axes q_1 and q_2, as in Figure 2. The helical content decreases gradually along the transition pathways, connecting the PrP^{C} isoform that has a high α-helical content to the PrP^{PU} conformation that has a low α-helical content. The α-helical contents were calculated by using the DSSP program.

In comparison with the two pathways on the wild-type energy landscape, the energy landscapes of the D178N and E200K mutants [Figs. 2(b) and (c), respectively) each contain only a single transition pathway connecting the PrP^C conformation with the PrP^{PU} regions. The pathways on the mutant energy landscapes, just like those on the wild-type energy landscape, are characterized by a decrease in the α-helical content when moving away from the PrP^C conformation [Figs. 3(b) and (c)]. Starting from the highly α-helical PrP^C isoform, the α-helical content decreases along the corresponding pathways from 46.7 to 23.0% in D178N and from 50.4 to 8.6% in E200K. The mere presence of two pathways on the wild-type PrP energy landscape, in comparison with the single pathway on the mutant energy landscapes, indicates that these two mutations indeed affect the mechanism of PrP^C conformational change. Furthermore, the differences in potential energies and in the helical content along the transition pathway of D178N versus that of E200K indicate that the two-point mutations affect the unfolding of the cellular prion protein in different ways.

Relative Stability of Individual PrP Helices

The PrP^C isoform of wild-type PrP, as well as those of its two mutants, contain the highest α-helical content among the sampled conformations. As discussed above, a significant decrease in the degree of helicity is found along the pathways toward their partially unfolded conformations (Fig. 3). It should be noted that the decrease in α-helical content along these transition pathways is not accompanied by an increase in the β-sheet content of the three PrP analogs. Rather, the helical regions turn into regions of random coil. Recently, a 10-ns MD simulation of monomeric PrP at 300 K and low pH using explicit solvent model for the water molecules showed a tendency of the N-terminal to form β-like structure.[30] However, these extended strands were not stable and did not form a true β-sheet motif. Four representative conformations are taken consecutively along each transition pathway (pathway I for wild-type PrP). These sets of conformations illustrate the unwinding of PrP^C helices 1, 2, and 3 along the transition pathways, moving from the PrP^C conformation to the partially unfolded isoforms, PrP^{PU}.

To help understand the characteristics of the specific conformation transitions in each protein, we present in Figure 4 the fractional lengths of the three helices projected on the two principal coordinates (q_1 and q_2) previously used for the description of the energy landscapes. The changes in the lengths of the three helices of wild-type PrP shown in Figure 4(a) indicate that greater structural changes occur along pathway I than pathway II. Furthermore, the unfolding of wild-type PrP^C along pathway I is characterized by an almost complete disappearance of helix 3, as well as by a significant unwinding of helix 2 (helix 1 is hardly affected). These characteristics are clearly captured by the four snapshots of Figure 5(a), demonstrating that only helix 1 remains in the partially unfolded PrP.

The changes in the lengths of the three helices in the D178N and E200K mutants are shown in Figures 4(b) and (c), respectively. Note that these figures reflect a dramatically different situation from that observed for wild-type PrP. In both mutants, helix 1 completely unwinds during the transition from PrP^C to PrP^{PU}. Helix 2 also significantly unwinds in both cases, whereas it is helix 3 that is least affected by the transition. The four consecutive D178N and E200K mutant conformations along the transition pathways shown in Figure 5(b) and (c), respectively, reflect this gradual unwinding of the helices, showing that only helix 3 remains in the partially unfolded isoform. Namely, both D178N and E200K mutations significantly affect the relative stability of the three PrP helices. The D178N and E200K substitutions significantly reduce the stability of helix 1, being the most stable helix in wild-type mouse PrP. The reverse is true with regard to the stability of helix 3. The two mutations significantly increase the stability of helix 3 in comparison to its relative instability in wild-type PrP.

Our observation is in accord with a recent MD study of PrP^C, which suggests that residues 109–175, which include helix 1, are much more mobile at low pH than at neutral pH and that the C-terminal helices (helices 2 and 3) are stable at both pH conditions.[30] It was also found that at low pH, helix 1 showed not only enhanced mobility but also experienced some loss of helicity at its C-terminus. The authors explained these observations as resulting from the protonation of the Asp, Glu, and His residues at low pH and the consequent breaking of salt-bridges involving these residues. Thus, the facilitated conformational changes of the prion protein at low pH and of D178N and E200K mutants are likely due to changes in the protonation state of ionizable residues, resulting in destabilizations of some hydrogen bonds and disruption of salt bridges.

The remarkable stability of wild-type PrP^C helix 1 (residues 144–156) and its intrinsic helical propensity were recently established by an NMR study of the PrP(143–158) peptide, which includes helix 1.[54] The self-stability of helix 1 was explained by Morrissey and Shakhnovich[55] by its high content of charged and hydrophilic residues, which make it one of the most soluble helices in the PDB. Namely, PrP^C helix 1 has a remarkably low capacity to form tertiary hydrophobic interactions and must instead be stabilized by internal electrostatic interactions. On the basis of the stability of isolated helix 1 in aqueous solution (as deduced from NMR measurements), it was hypothesized that helix 1 would be preserved during the conformational transition from PrP^C to PrP^{SC}.[54] On the other hand, on the basis of the highly unusual hydrophilicity and charge distribution of helix 1, it was proposed that prion infectivity may involve unraveling of helix 1. This will be the rate-limiting step of the prion pathogenic transition, before forming a β-aggregate of constituent helix 1 components that is stabilized by salt bridges.[55] The latter model predicts that several point mutations may destabilize PrP^C helix 1 and, consequently, accelerate its unraveling.

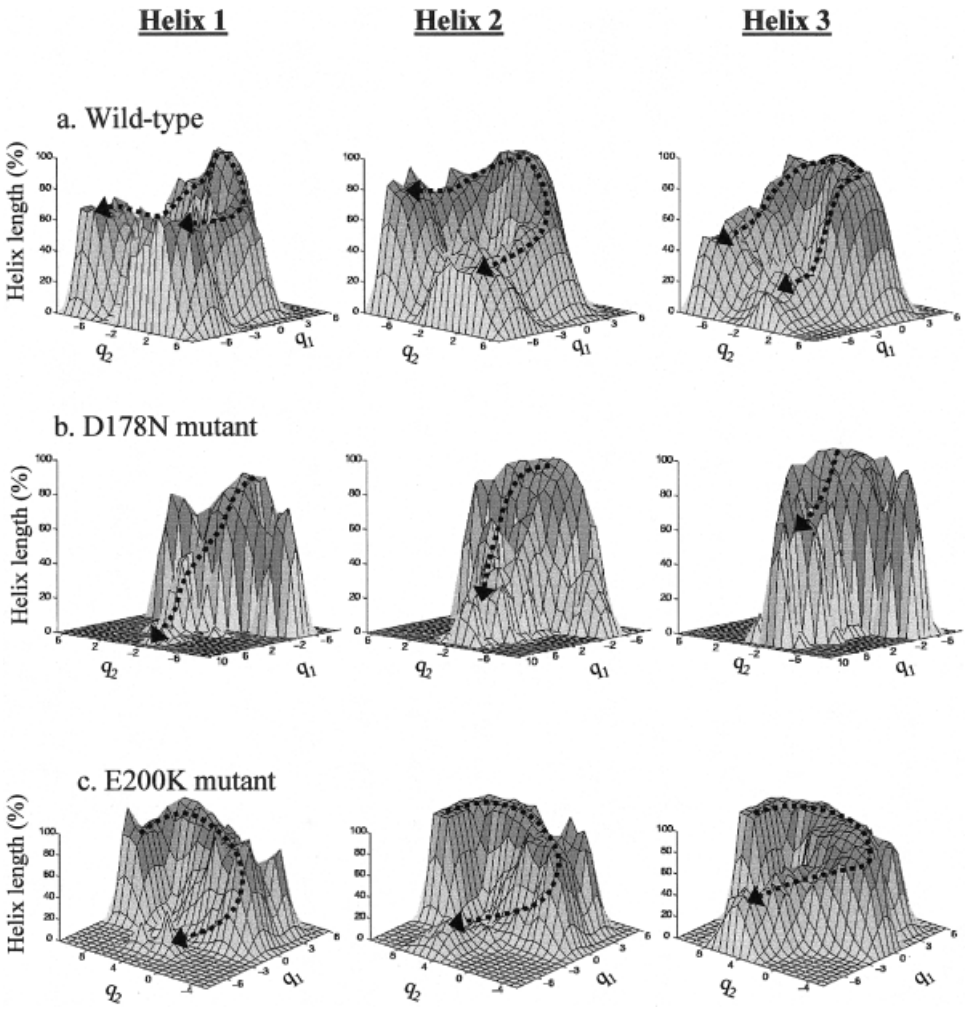

Fig. 4. The fractional lengths of the three PrP^C helices for all sampled conformations of (**a**) wild-type PrP, (**b**) D178N mutant, and (**c**) E200K mutant projected on the two principal coordinates, axes q_1 and q_2, as in Figure 2. The maximal lengths (100%) of helices 1, 2, and 3 are 13 residues (144–156), 23 residues (173–194), and 22 residues (200–228), respectively (see Materials and Methods).

Our results support the intrinsic helical propensity of helix 1, as well as its destabilization due to the mutations as previously proposed.[54,55] Moreover, even though our study deals with a single PrP molecule, it may indicate that helix 1 plays a central role in prion aggregation, as suggested by the model for prion infectivity discussed above.[55] That model suggests that PrP^{SC} is an aggregate with a hydrophilic core, consisting of a β-sheet-like arrangement of constituent helix 1 components. Therefore, the lesser stability of helix 1 that we find in the mutants may indicate a smaller energetic barrier for the unwinding of this helix, consequently, aiding the appearance of CJD.

Properties of Wild-Type and Mutant PrP^C and PrP^{PU} Isoforms

The average stability and structural properties of the PrP^C isoform of wild-type PrP and those of the D178N and E200K mutants are summarized in Table I. A comparison between the effect of the two mutations on the wild-type PrP^C conformations indicates that both mutations affect the stability and the structure of PrP^C; however, their effect is not identical. Energetically, the D178N substitution destabilizes the PrP^C to a larger extent than the E200K substitution. The D178N mutation destabilizes the PrP^C state by about 26 kcal/mol, whereas the E200K substitution destabilizes it only by 16 kcal/mol. The larger destabilization, due to the D178N mutation, can be explained by the loss of a hydrogen bond (Tyr128-Asp178) and of a salt bridge (Arg164-Asp178) when substituting Asp by Asn (see Fig. 1). On the basis of site-directed mutagenesis and urea-induced equilibrium transition experiments, it was found that the D178N mutant is 1.7 kcal mol^{-1} less stable than wild-type PrP.[56] The difference of one order of magnitude between the experimental and the simulation result for the destabilization by the D178N mutation reflects the crude approximations involved in the treatment of charged residues in the EEF1 model. According to this study and the aforementioned 300 K MD

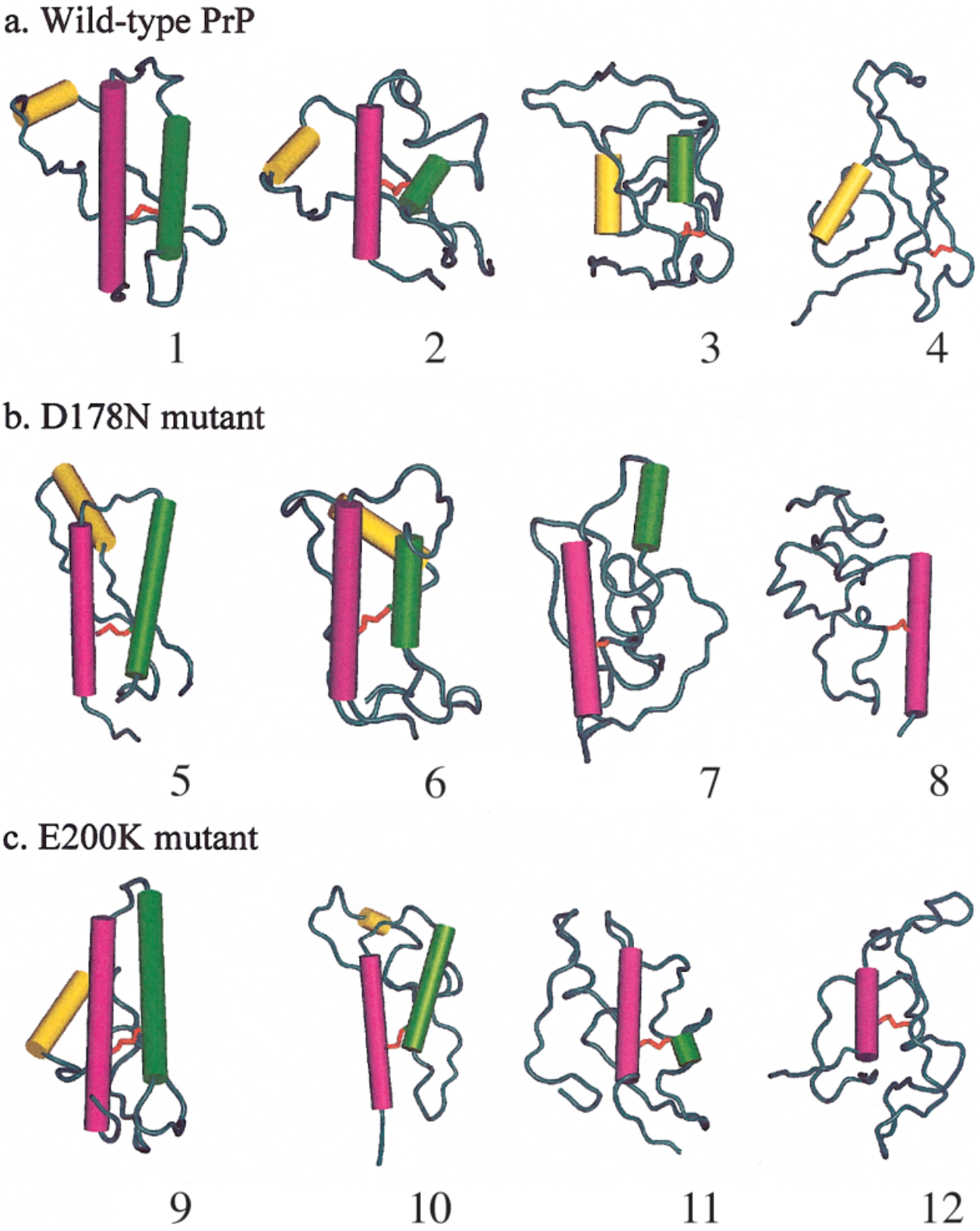

Fig. 5. Four PrP conformations sampled along a transition pathway connecting the PrP^{C} conformation region to the PrP^{PU} conformation region.for (**a**) wild-type PrP, (**b**) D178N mutant, and (**c**) E200K mutant. Points 1–4, 5–8, and 9–12 are indicated on the corresponding energy landscapes in Figure 2. The path from the PrP^{C} structures (1, 5, and 9) to the partially unfolded PrP structures (4, 8, and 12) reveals a gradual unwinding of the wild-type PrP^{C} α-helices. Although only helix 1 remains in the wild-type PrP^{PU}, both mutant PrP^{PU} are characterized by a trace of helix 3. As in Figure 1, helix 1 is marked in yellow, helix 2 in green, helix 3 in pink, and the disulfide bond in red.

TABLE I. Average Properties of the Native PrP^C Isoforms of Wild-Type PrP and of Its D178N and E200K Mutants[†]

	Wild-type	D178N	E200K
Stability			
Self energy[a] (kcal/mol)	−3433 ± 7	−3416 ± 20	−3424 ± 33
Solvation energy[b] (kcal/mol)	−1010 ± 5	−1001 ± 19	−1003 ± 32
Total energy[c] (kcal/mol)	−4443 ± 2	−4417 ± 3	−4427 ± 1
Structure			
% α-helix[d]	44.8 ± 2.4%	43.7 ± 7.2%	45.8 ± 12.5%
% β-sheet[d]	3.4 ± 2.5%	4.8 ± 3.3%	2.2 ± 2.4%
Length of helix 1[e]	6.5 ± 0.7 a.a. (59.2 ± 11.3%)	7.3 ± 1.4 a.a. (66.9 ± 18.9%)	6.5 ± 1.4 a.a. (59.4 ± 21.7%)
Length of helix 2[e]	19.5 ± 1.5 a.a. (84.7 ± 7.7%)	15.7 ± 3.8 a.a. (68.3 ± 24.2%)	19.3 ± 5.4 a.a. (84.0 ± 28.3%)
Length of helix 3[e]	18.6 ± 0.9 a.a. (84.5 ± 4.8%)	19.0 ± 1.5 a.a. (86.4 ± 7.9%)	19.6 ± 3.6 a.a. (89.3 ± 18.2%)
Radius of gyration (Å)	14.4 ± 0.1	15.3 ± 0.7	14.5 ± 0.4

[†]The averages were calculated over the 50 conformations with the lowest total energy.
[a]CHARMM potential energy.
[b]EEF1 implicit solvation energy.
[c]The sum of the self-energy and the solvation energy.
[d]Calculated by the DSSP program.
[e]Helix length in number of amino acids (left) and in percentage relative to the maximal lengths of these helices (right). The maximal lengths of helices 1, 2, and 3 as found in the conformation samples were 11, 23, and 22 residues, respectively.

simulation study,[30] it was predicted that this mutation will facilitate the conversion to PrP^{SC}. This effect is not present in the E200K mutation, which does not involve any loss of stabilizing intramolecular interactions. The main source for destabilization in the E200K mutant is different interactions of Lys and Glu with the solvent.

Structurally, the lengths of the three helices that make up the PrP^C isoform are not identical in the wild-type and in the two mutants, even though the average α-helical contents are very similar for the three analogs (between 43.7 and 45.8%). The larger variance values for the helix lengths in the mutants indicate lower stability for these secondary structure elements in comparison to their stability in the wild-type. As predicted above, based on the different location of the two mutations (positions 178 and 200), the structural properties of the two PrP^C mutants are also different from one another. Although the average lengths of the PrP^C helices in the E200K mutant are similar to those of the wild-type, significant differences in the secondary structure are observed for the D178N mutant. In this mutant, helix 1 contains about 7.3 residues, whereas in the wild-type and in the E200K PrP^C, it is shorter by one residue. Most important, in D178N PrP^C, helix 2 is composed of 15.7 residues in comparison to 19.3 and 19.5 residues for wild-type and E200K mutant PrP^C, respectively. The dramatic destabilization of D178N PrP^C helix 2 is because this substitution position is located in that helix and involves the loss of a hydrogen bond and of a salt bridge. The disruption of helix 2 in D178N leads to an increase in the radius of gyration of PrP^C isoform from 14.5 Å in the wild-type and E200K mutants to 15.3 Å in the D178N mutant.

The average properties of the partially unfolded PrP isoform, denoted here as PrP^{PU}, of wild-type PrP and of the two mutants, are summarized in Table II. For all three PrP analogs, the PrP^{PU} isoform is less stable than the PrP^C isoform. This destabilization amounts to about 55, 54, and 39 kcal/mol compared to PrP^C for wild-type, D178N, and E200K mutants, respectively. The secondary structure elements of the PrP^{PU} isoforms are related to those of PrP^C; however, they are fewer and shorter as indicated by the significantly lower α-helical contents and the lengths of the three helices. In the wild-type partially unfolded PrP, only small fragments of helices 1 and 2 remain and no traces of helix 3 are found. In the mutants, different helices are found at the partially unfolded state. For both D178N and E200K mutants, helix 3 is still found in the partially unfolded isoform, but only in the D178N mutant one also finds a remaining fragment of helix 2.

Comparing the mutations' effect on both native PrP^C and PrP^{PU} isoforms indicates that both mutations affect the relative stability of the three helices. Although in wild-type PrP the stability of helix 1 is the greatest and the stability of helix 3 is the smallest, there is an inversion in their relative stability due to the mutations. Note that, although the relative stability of the three helices is similar in the two mutants, their energy landscapes suggest that their unfolding mechanisms will be different [Figs. 2(b) and (c)].

The destabilization of helix 1 in the mutants is due to the changes in the charge distribution that affects the self-electrostatic interactions (i.e., internal salt bridges) of helix 1. In the case of the D178N mutation, a negatively charged residue is substituted by uncharged hydrophilic residues and in the case of E200K a negatively charged residue is substituted by a positively charged residue. The E200K mutation may destabilize helix 1 directly because it is adjacent to it (Fig. 1). However, the D178N destabilizes helix 1 indirectly through changes in the intermolecular interactions of residue 178 with Tyr128 and Arg164 (Fig. 1), which affect the self-electrostatic interactions that stabilize helix 1. Recently, it was proposed on the basis of detailed MD study of wild-type PrP at low pH that neutralization of Asp178 (by mutation to Asn or by protonation) may result in breaking the interaction with Tyr128.[30] The lack of this interaction makes Tyr128 free to move and may affect with the assistance of other residues the chemical environment of helix 1. These results may

TABLE II. Average Properties of PrP^{PU} Isoforms of Wild-Type PrP and Its D178N and E200K Mutants[†]

	Wild-type	D178N	E200K
Stability			
Self energy[a] (kcal/mol)	−3311 ± 27	−3309 ± 33	−3307 ± 22
Solvation energy[b] (kcal/mol)	−1077 ± 21	−1053 ± 27	−1080 ± 21
Total energy[c] (kcal/mol)	−4388 ± 16	−4363 ± 17	−4388 ± 19
Structure			
% α-helix[d]	8.6 ± 1.3%	18.5 ± 1.9%	6.0 ± 2.1%
% β-sheet[d]	0.4 ± 1.1%	0.3 ± 1.2%	1.8 ± 2.6%
Length of helix 1[e]	5.1 ± 0.6 a.a. (46.1 ± 11.8%)	0 a.a. (0%)	0 a.a. (0%)
Length of helix 2[e]	2.7 ± 0.2 a.a. (11.9 ± 7.4%)	4.6 ± 0.5 a.a. (20.0 ± 11.5%)	0.4 a.a. (1.7 ± 5.3%)
Length of helix 3[e]	0 a.a. (0%)	13.2 ± 1.3 a.a. (60.1 ± 9.5%)	6.2 ± 0.6 a.a. (28.1 ± 9.7%)
Radius of gyration (Å)	14.8 ± 0.8	16.5 ± 1.4	15.5 ± 0.7

[†]For wild-type and E200K mutant PrP, the averages were calculated over conformations with α-helical content <10% (11 and 60 conformations for wild-type and E200K mutant, respectively). For D178N mutant, the averages were calculated over conformations with α-helical content <20% (12 conformations).
[a]CHARMM potential energy.
[b]EEF1 implicit solvation energy.
[c]The sum of the self-energy and the solvation energy.
[d]Calculated by the DSSP program.
[e]Helix length in number of amino acids (left) and in percentage relative to the maximal lengths of these helices (right). The maximal lengths of helices 1, 2, and 3 as found in the conformation samples were 11, 23, and 22 residues, respectively.

suggest that other known PrP mutations that do not involve a marked change in hydrophilicity will affect differently the structure of PrP^C and the mechanism of the structural conversion.

CONCLUSIONS

Mapping the energy landscapes of three prion protein analogs, the wild-type and two mutants, enabled the characterization of a PrP conformational transition, which is characterized by a decrease in the α-helical content. In particular, it was found that: (i) the PrP^C isoform of the D178N and E200K mutant PrPs is less stable than the wild-type native PrP^C isoform; (ii) two transition pathways are observed for the unfolding of wild-type PrP^C, whereas the energy landscapes of the D178N and E200K mutants reflect a single transition pathway; (iii) the effects of the two mutations on the wild-type PrP^C are not identical because (a) the D178N PrP^C is less stable than the E200K PrP^C; (b) although the lengths of the three helices of E200K PrP^C are very similar to those of the wild-type PrP^C, the lengths of helix 1 and helix 2 of the D178N PrP^C are different from those of the wild-type PrP^C; and (c) the single transition pathway of the energy landscapes of the two mutants indicates a different unfolding mechanism; (iv) helix 1 is the most stable helix in wild-type PrP and it remains in the partially unfolded conformations. In the two mutants, the stability of helix 1 is dramatically reduced and helix 3 becomes the most stable helix.

The remarkable stability of helix 1 in wild-type PrP^C, which was found in the present study, was recently established by an NMR study of the PrP(143–158) peptide[54] and was explained as a consequence of its high content of charged and hydrophilic residues, making it one of the most soluble helices in the PDB.[55] The destabilization of helix 1 as a result of the D178N and E200K point mutations is due to changes in charge distribution that affects the internal salt bridges of helix 1. A similar effect was recently observed at low pH where protonated Asp, Glu, and His were not likely to form electrostatic interactions.

The destabilization of helix 1, due to the D178N and E200K point mutations, supports the model for the prion infectivity proposed by Morrissey and Shakhnovich.[55] Their model proposes that PrP^{SC} is an aggregate with a hydrophilic core, consisting of a β-sheet-like arrangement of constituent helix 1 components. Accordingly, the destabilization of helix 1 in the mutants PrP results in a smaller energetic barrier for the unwinding of this helix and, consequently, accelerated the appearance of CJD.

Our study indicates that the unfolding processes of the PrPs are characterized by a gradual and hierarchical unwinding of the three helices, and no formation of β-sheet elements that define the PrP^{SC} isoform was probed. The latter observation might be due to thermodynamic and kinetic reasons. Namely, it is suggested that a monomeric PrP^{SC} is not stable in solution and that relative high energetic and entropic barriers separate it from the rest of the landscape. Accordingly, longer simulation of isolated monomeric PrP should be carried out to detect accumulation of β-sheets. Alternatively, it is possible that β-sheet formation is coupled with the association of several PrP subunits[57] and is not a question of the simulation length. In the language of energy landscapes, fusing two landscapes of monomeric PrP to form the energy landscape of dimeric PrP may result in stabilization of PrP^{SC} and lower barriers. It is also possible that the flexible N-terminal region (residues 1–122) or the oligosaccrides at the two glycosylation sites (Asn181IleThr and Asn197PheThr) may increase the stability of monomeric PrP^{SC}. We would like to note that although the EEF1 implicit solvent model has been shown to give good results in a variety of applications and was found to yield a good agreement with explicit solvent simulations, the approximations involved in its

potential function, such as the treatment of the electrostatic screening by approximating distance-dependent dielectric function and the neutralization of ionic groups, might distort the relative energies. The inaccuracies of the implicit solvent model may provide another possible explanation for the absence of β-sheet elements in the current study.

The simulations of the isolated monomeric PrPs presented here reflect the internal flexibility of the PrP^{C} and the relative stability of the secondary structure units. This approach can reveal the importance of each secondary structure element on the pathogenic conversion and the effect of point mutations on its stability before formation of β-sheets, presumably due to association. However, the current results cannot fully support neither the catalytic nor the nucleated polymerization models of PrP infection. On the one hand, the partially unfolded PrP state (PrP^{PU}) found in this study may correspond to the hypothetical transitional PrP* isoform that was suggested as playing a key role in the catalytic model of prion infection. To elucidate the stability of β-sheets elements in a monomeric prion protein, a better electrostatic model should be used. On the other hand, the fact that β-sheet elements were not detected in this partially unfolded state of the PrP may support the nucleated polymerization model that proposes that PrP^{SC} is intrinsically multimeric and an observation of β-sheet elements is correlated with the aggregation of PrP molecules. Accordingly, to detect PrP^{SC} MD simulations should take explicitly or implicitly into account the intermolecular interactions responsible for the formation of prion aggregates.

REFERENCES

1. Prusiner SB. Novel proteinaceous infectious particles cause scrapie. Science 1997;278:245–251.
2. Prusiner SB, Scott MR, DeArmond SJ, Cohen FE. Prion protein biology. Cell 1998;93:337–348.
3. Caughey B, Chesebro B. Prion protein and the transmissible spongiform encephalopathies. Trends Cell Biol 1997;7:56–62.
4. Harrison PM, Bamborough P, Daggett V, Prusiner SB, Cohen FE. The prion protein problem. Curr Opin Struct Biol 1997;7:53–59.
5. Aguzzi A, Weissmann C. Prion research: the next frontiers. Nature 1997;389:795–798.
6. Chesebro B. BSE and prions: uncertainties about the agent. Science 1998;279:42–43.
7. Pan K, Baldwin M, Nguyen J, Gasset M, Groth D, et al. Conversion of α-helices into β-sheets features in the formation of the scapie prion proteins. Proc Natl Acad Sci USA 1993;90:10962–10966.
8. Safar J, Roller PP, Gajdusek DC, Gibbs CJ. Scrapie amyloid (prion) has the conformational characteristics of an aggregated molten globule folding intermediate. Biochemistry 1994;33:8375–8383.
9. Riek R, Hornemann S, Wider G, Glockshuber R, Wuthrich W. NMR characterization of the full-length recombinant murine prion protein, mPrP(23–231). FEBS Lett 1997;413:282–288.
10. Riek R, Hornemann S, Wider G, Billeter M, Glockshuber R, Wuthrich W. NMR structure of the mouse prion protein domain PrP(121–231). Nature 1996;382:180–182.
11. James TL, Liu H, Ulyanov NB, Farr Jones S, Zhang H, et al. Solution structure of a 142-residue recombinant prion protein corresponding to the infectious fragment of the scrapie isoform. Proc Natl Sci Acad USA 1997;94:10086–10091.
12. Garcia FL, Zahn R, Riek R, Wuthrich K. NMR structure of the bovine prion protein. Proc Natl Acad Sci USA 2000;97:8334–8339.
13. Zahn R, Liu A, Luhrs T, Riek R, Schroetter CV, Garcia FL, Billeter M, Calzolai L, Wider G, Wuthrich K. NMR solution structure of the human prion protein. Proc Natl Acad Sci USA 1999;97:145–150.
14. Kelly JW. Mechanisms of amyloidogenesis. Nat Struct Biol 2000;7:824–826.
15. Huang Z, Prusiner SB, Cohen FE. Scarpie prions: a three-dimensional model of an infectious fragment. Fold Design 1996;1:13–19.
16. Telling GC, Scott M, Mastrianni J, Gabizon R, Torchia M, Cohen FE, DeArmond SJ, Prusiner SB. Prion propagation in mice expressing human and chimeric PrP transgenes implicates the interaction of cellular PrP with another protein. Cell 1995;83:79–90.
17. Lansbury PT, Caughey B. The chemistry of scrapie infection: implications of the "ice 9" metaphor. Chem Biol 1995;2:1–5.
18. Caughey B, Kocisko DA, Raymond GJ, Lansbury PT. Aggregates of scrapie-associated prion protein induce the cell-free conversion of protease-sensitive prion protein to the protease-resistant state. Chem Biol 1995;2:807–816.
19. Kelly JW. The alternative conformations of amyloidogenic proteins and their multi-step assembly pathways. Curr Opin Struct Biol 1998;8:101–106.
20. Huang Z, Prusiner SB, Cohen FE. Structures of prion proteins and conformational models for prion diseases. Curr Top Microbiol Immunol 1996;207:49–67.
21. Huang Z, Gabriel J-M, Baldwin MA, Flettrick RJ, Prusiner SB, Cohen FE. Proposed three-dimensional structure for cellular prion protein. Proc Natl Acad Sci USA 1994;91:7319–7143.
22. Riek R, Wider G, Billeter M, Hornemann S, Glockshuber R, Wuthrich W. Prion protein NMR structure and familial human spongiform encephalopathies. Proc Natl Acad Sci USA 1998;95:11667–11672.
23. Levy Y, Hanan E, Solomon B, Becker OM. The helix-coil transition of PrP106–126: a molecular dynamic study. Proteins 2001;45:382–396.
24. Goldfarb L, Korczyn A, Brown P, Chapman J, Gajdusek DC. Mutation in codon 200 of scrapie amyloid precursor gene linked to Creutzfeldt-Jacob disease in Sephardic of Libyan and non-Libyan origin. Lancet 1990;336:637.
25. Goldfarb LG, Petersen RB, Tabaton M, Brown P, LeBlanc AC, et al. Fatal insomnia and familial Creutzfeldt-Jakob disease: disease phenotype determined by a DNA polymorphism. Science 1992;258:806–808.
26. Hsiao K, Meiner Z, Kahana E, Cass C, Kahana I, et al. Mutation of the prion protein on Libyan Jews with Creutzfeldt-Jakob disease. N Engl J Med 1991;324:1091.
27. Zuegg J, Gready JE. Molecular dynamics simulations of human prion protein: Importance of correct treatment of electrostatic interaction. Biochemistry 1999;38:13862–13876.
28. Parchment O, Essex J. Molecular dynamics of mouse and syrian hamster PrP: implications for activity. Proteins 2000;38:327–340.
29. Guilbert C, Richard F, Smith JC. Dynamic simulation of the mouse prion protein. Biopolymers 2000;54:406–415.
30. Alonso DOV, DeArmond SJ, Cohen F, Daggett V. Mapping the early steps in the pH-induced conformational conversion of the prion protein. Proc Natl Acad Sci USA 2001;98:2985–2989.
31. Gsponer J, Ferrara P, Caflisch A. Flexibility of murine PrP and its Asp178Asn mutant investigated by molecular dynamics simulations. J Mol Graph Mod 2001;20:169–182.
32. Frauenfelder H, Sliger SG, Wolynes PG. The energy landscapes and motions of proteins. Science 1991;254:1598–1603.
33. Onuchic JN, Luthey-Schulten Z, Wolynes PG. Theory of protein folding: the energy landscape perspective. Annu Rev Phys Chem 1997;48:539–594.
34. Frauenfelder H, McMahon B. Energy landscape and fluctuations in proteins. Ann Phys (Leipzig) 2000;9:655–667.
35. Levy Y, Becker OM. Wild-type and mutant prion proteins: insights from energy landscape analysis. In: Solomon B, Taraboulos A, Katchalski-Katzir E, editors. Conformational diseases—a compendium. Jerusalem: Bialik Institute; 2001. p 97–102.
36. Becker OM. Principal coordinate maps of molecular potential energy surfaces. J Comp Chem 1998;19:1255–1267.
37. Becker OM. Geometric versus topological clustering: an insight into conformation mapping. Proteins 1997;27:213–226.
38. Levy Y, Becker OM. Energy landscapes of conformationally constrained peptides. J Chem Phys 2001;114:993–1009.
39. Brooks BR, Bruccoleri RE, Olafson BD, States DJ, Swaminathan S, Karplus M. CHARMM: a program for macromolecular energy, minimization and dynamic calcualtion. 1983;4:187–217.

40. MacKerell AD Jr, Bradhford D, Bellot M, Dubrack RL Jr, Evanseck JD, et al. All-atom empirical potential for molecular modeling and dynamics studies of proteins. J Phys Chem B 1998;102:3586–3616.
41. Lazaridis T, Karplus M. Effective energy function for proteins in solution. Proteins 1999;35:133–152.
42. Dinner AR, Lazaridis T, Karplus M. Understanding β-hairpin folding. Proc Natl Acad Sci USA 1999;96:9068–9073.
43. Kumar S, Sham YY, Tsai C-J, Nussinov R. Protein folding and function: the N-terminal fragment in adenylate kinase. Biophys J 2001;80:2439–2454.
44. Tsai C-J, Ma B, Sham YY, Kumar S, Nussinov R. Structured disorder and conformational selection. Proteins 2001;44:418–427.
45. Paci E, Karplus M. Forced unfolding of fibronectin type 3 modules: an analysis by biased MD simulations. J Mol Biol 1999;288:441–449.
46. Inuzuka Y, Lazaridis T. On the unfolding of α-lytic protease and the role of the Pro region. Proteins 2000;41:21–32.
47. Lazaridis T, Karplus M. Discrimination of the native from misfolded protein models with an energy function including implicit solvation. J Mol Biol 1999;288:477–487.
48. Lazaridis T, Karplus M. Effective energy functions for protein structure prediction. Curr Opin Struct Biol 2000;10:139–145.
49. Petrella RL, Karplus M. A limiting-case study of protein structure prediction: energy-based searches of reduced conformational space. J Phys Chem B 2000;104:11370–11378.
50. Lazaridis T, Karplus M. "New view" of protein folding reconciled with the old through multiple unfolding simulations. Science 1997;278:1928–1931.
51. Levy Y, Jortner J, Becker OM. Solvent effects on the energy landscapes and folding kinetics of polyalanine. Proc Natl Acad Sci USA 2001;98:2188–2193.
52. Becker OM. In computational biochemistry and biophysics. New York: Marcel Dekker; 2001.
53. Kabsch W, Sander C. Dictionary of protein secondary structure: pattern recognition of hydrogen-bonded and geometrical features. Biopolymers 1983;22:2577–2637.
54. Liu A, Riek R, Zahn R, Hornemann S, Glockshuber R, Wuthrich K. Peptides and proteins in neurodegenerative disease: helix propensity of a polypeptide containing helix 1 of a mouse prion protein studied by NMR and CD spectroscopy. Biopolymers 1999;51:145–152.
55. Morrissey MP, Shakhnovich EI. Evidence for the role of PrP^C helix in the hydrophilic seeding of prion aggregates. Proc Natl Acad Sci USA 1999;96:11293–11298.
56. Liemann S, Glockshuber R. Influence of amino acid substitutions related to inherited hyman prion diseases on the thermodynamic stability of the cellular prion proetin. Biochemistry 1999;38:3258–3267.
57. Soto C. Protein misfolding and disease; protein refolding and therapy. FEBS Lett 2001;498:204–207.